# Interaction of neutrons with even-$A$ tin isotopes: Neutron-excess dependence in scattering at $E_n = 1.00$ and 1.63 MeV

R. W. Harper, J. L. Weil, and J. D. Brandenberger*
*Department of Physics and Astronomy, University of Kentucky, Lexington, Kentucky 40506*
(Received 12 March 1984)

Differential cross sections have been measured with unusually good precision and accuracy for neutrons scattered from samples of $^{116,118,120,122,124}$Sn using a time-of-flight spectrometer. Measurements were made at two bombarding energies to look for effects of the number of exit channels on the scattering: 1.00 MeV, where the scattering is all elastic, and 1.63 MeV, where both elastic and inelastic scattering can occur. The elastic-scattering data have root mean square relative and normalization uncertainties, respectively, of 2.7—5.5 % and 1.8%; for the inelastic-scattering data these uncertainties are 4.7—6.3 % and 4.5%, respectively. The angular distributions for elastic scattering vary systematically with neutron excess. The elastic-scattering cross sections were fitted together with total cross sections using an incoherent sum of shape-elastic scattering, calculated with a complex spherical potential, and compound-elastic scattering, calculated with a statistical model using the same potential. The real and imaginary well depths have been parametrized as linear functions of neutron excess. A strong neutron-excess dependence of $W$ is required to fit the data. For $R = r_0 A^{1/3}$, the results at 1.00 MeV are $V = 52.42 - 28.6(N-Z)/A$ MeV and $W = 14.38 - 51.0(N-Z)/A$ MeV, and the results at 1.63 MeV are $V = 51.41 - 29.5(N-Z)/A$ MeV and $W = 11.75 - 34.1(N-Z)/A$ MeV. The neutron-excess dependence of $V$ and $W$ on the rate of change of radius versus $A$ has been investigated, as well as the effects on $V$ and $W$ of an overall change in geometrical parameters. The neutron-excess dependence of $V$ is strongly dependent on the $R$ versus $A$ relation.

## I. INTRODUCTION

The famous review papers of Feshbach[1,2] offer a theoretical foundation for a complex potential description of energy-averaged neutron scattering cross sections for a particular nucleus. Fixing the parameters of a scattering potential with minimum ambiguity is the first step toward being able to see the effects of the nuclear structure of the target on the scattering.

However, in going from one nucleus to another, it is difficult to tell whether changes in the observed scattering should be ascribed to systematic changes in the potential or to differences in nuclear structure between the two nuclei. Separating systematic properties of neutron scattering from nuclear structure influences requires comparisons of scattering from several nuclei. The even-$A$ tin isotopes are an excellent set for testing systematic effects of neutron excess, since the nuclear structures of all of them are quite similar, as discussed in more detail in a companion study[3] to that reported here.

The present work is the second in a series reporting on the results of an experimental investigation into the neutron excess dependence of the optical potential parameters which describe low energy neutron-nucleus scattering, both elastic and inelastic. This study focuses on the effect of adding successive pairs of neutrons over a limited range of mass number with the aim of comparing the result with the neutron-excess dependence found in global analyses.[4]

One of the most important problems in studying scattering systematics is the ambiguity introduced by uncertainties in potential parameters other than the ones of most immediate interest. To avoid such ambiguities in the potential, precise and accurate measurements of several scattering observables are needed. The most important measurable quantities for fixing potentials other than elastic-scattering data are total cross sections, the subject of the first paper[3] in this series. A basic source of ambiguity for scattering potentials is the separation of the fluctuation, or absorption, cross section from that for direct scattering. The contribution of the fluctuation cross section to the elastic scattering, e.g., the compound elastic, is strongly influenced by the number of open channels.[5,6] For this reason, and to attempt to see the effects of the number of scattering channels on the potential, we have made measurements at incident energies of 1.00 and 1.63 MeV. At 1.00 MeV only elastic scattering is possible, since that energy is just below the energy of the $2^+$ first excited state. At 1.63 MeV the number of open exit channels is doubled with the onset of inelastic scattering to the $2^+$ state. A comparison of analyses at these two energies might reveal an influence of the onset of inelastic scattering on the scattering potentials, if any noticeable effect occurs.

We have measured differential cross sections for the elastic scattering of 1.00 MeV neutrons and for the elastic and inelastic scattering of 1.63 MeV neutrons from enriched-isotope samples of $^{116,118,120,122,124}$Sn. All previous measurements on tin in this energy range[7–9] used natural tin as a scattering sample. Similar measurements have been made on tin isotopes at neutron energies of 11 and 24 MeV for the purpose of studying the neutron ex-

 

TABLE I. Time-of-flight experimental details.

| | | |
|---|---|---|
| Neutron bombarding energy | 1.00 MeV | 1.63 MeV |
| Energy spread (FWHM) | 118 keV | 98 keV |
| Flight path | 2.21 m | 1.93 m |
| Neutron source-to-scattering sample distance | 9.5 cm | 8.8 cm |
| Photomultiplier tube | 58 AVP | RCA 8854 |
| Neutron detection threshold | 250 keV | $<50$ keV |
| Angular range of data | 30°–153.5° | 20°–153° |
| Proton energy loss in foil | 261 keV | 197 keV |
| Proton energy loss in gas | 110 keV | 90 keV |

cess dependence.[10] A special feature of the measurements reported here is their unusually high precision and accuracy. This is due, at least in part, to the use of the isotopic total cross sections[3] for normalization, which reduced the normalization uncertainty by about a factor of 2 compared to more usual methods of normalizing to other differential cross sections.

## II. EXPERIMENTAL APPARATUS

Neutron scattering differential cross sections were measured using a neutron time-of-flight (TOF) spectrometer. The University of Kentucky 6.5 MV Van de Graaff accelerator was used to produce monoenergetic neutrons from the $^3$H(p,n)$^3$He reaction. The proton beam was pulsed in the terminal at a rate of 2 MHz with a pulse width of 8 ns, and passed through a 3.6 $\mu$m thick molybdenum foil into a 3.0 cm long by 0.8 cm diam cylindrical gas cell made of thin-walled stainless steel. The cell was lined with 0.025 cm thick tantalum and contained tritium gas at 1.0 atm pressure. Proton straggling in the foil and gas was assumed to follow the Vavilov[11] distribution and was calculated using the tables of Seltzer and Berger.[12] Neutrons emitted at 0° had mean energies of 1.00 or 1.63 MeV. The scattering samples were cylinders of metallic tin; their dimensions and isotopic composition are given in Table I of Ref. 3.

The experimental apparatus was similar to that of Ref. 13, except that no intermediate detector shield was used. A massive $Li_2CO_3$-loaded paraffin detector shield, mounted on a goniometer, was used to reduce the room-scattered background, the neutron background from the source, and other backgrounds. The neutron detector was a NE 218 liquid scintillator 11.1 cm in diameter by 1.3 cm thick, coupled to a 58 AVP or RCA 8854 photomultiplier tube. A neutron monitor, which was also operated in the TOF mode, was mounted above the scattering plane 5.2 m from the source at an angle of 25 deg to the beam axis. The monitor was a 2.5 cm diam by 4.0 cm thick plastic scintillator on a 56 AVP photomultiplier in a $Li_2CO_3$-loaded paraffin shield, tightly collimated to view the source directly. Other details of the experimental setups at the two bombarding energies are given in Table I.

The main and monitor detector electronics systems were standard TOF systems with fast timing pulses from phototube anodes timed with respect to the beam pulses. A pulse-height bias was set for each detector by a discriminator circuit whose input was the linearly amplified dynode signal and whose output was used to gate acquisition of the TOF spectrum. The electronics for both detectors was essentially the same as is shown in Ref. 13, except that the pulse-shape discrimination and dynamic biasing features used there were not used in the present experiment. To determine the low-energy cutoff of the detector, a discriminator on the linear signal from the dynode was set in the valley of the spectrum of the 59.5 keV $\gamma$ ray of $^{241}$Am for each detector, except the main detector in the 1.63 MeV experiment, for which the discriminator was set at half this value. Further details on the experimental apparatus can be found in Refs. 13–15.

## III. EXPERIMENTAL PROCEDURES

### A. Data collection and reduction

The energy dependence of the detection efficiency of the neutron detector was determined by measuring the angular distribution of the $^3$H(p,n)$^3$He reaction at several proton energies and comparing yields to the values in the tabulation of Liskien and Paulsen.[16] The efficiency curve used at 1.63 MeV bombarding energy is shown in Fig. 1, and is similar, except for the low energy cutoff, to that for the 1.0 MeV data.

Scattering samples were suspended a short distance from the tritium cell on the axis of the incident proton beam. TOF spectra of the scattered neutrons were measured with and without a scattering sample. The sample-

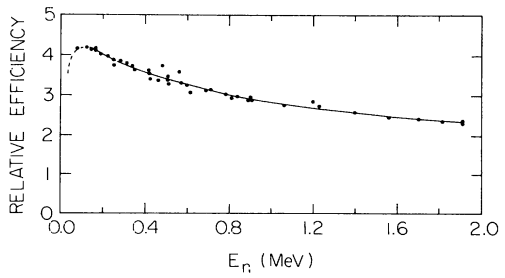


FIG. 1. The measured relative efficiency of the neutron detector used in the 1.63 MeV measurements as a function of neutron energy. The efficiency curve for the 1.00 MeV measurements had a cutoff at 0.30 MeV.

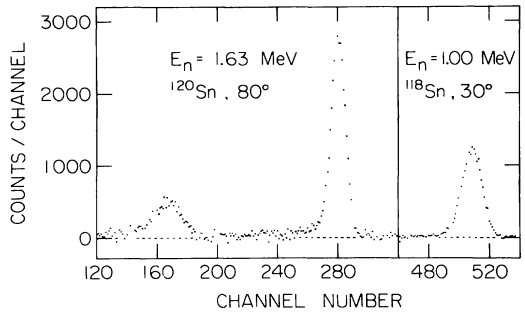


FIG. 2. Typical TOF spectra after background subtraction.

out TOF spectra were subtracted channel by channel from the sample-in spectra, and then residual backgrounds were estimated and subtracted. Typical spectra are shown in Fig. 2. TOF spectra were also recorded for the monitor detector and the time-independent background was subtracted to determine the neutron yield. All yields were corrected for the dead time of the ADC's, which was 1—4 %. The main detector yields were also corrected for the energy dependence of the detection efficiency. Statistical uncertainties in the monitor yields were $<1\%$.

### B. Finite geometry corrections

At both bombarding energies, neutron scattering is the only significant process. Hence the angle-integrated elastic cross section at 1.0 MeV should agree with the total neutron cross section at that energy and, at 1.63 MeV, the sum of the angle-integrated elastic and inelastic scattering cross sections should agree with the total cross section. The total cross sections of these isotopes in this energy region have been measured[3] in this laboratory and were used to normalize the differential scattering cross sections.

Flux attenuation in the sample and neutron source anisotropy over the solid angle subtended by the sample cause an angle independent reduction in scattered yields from that expected in the ideal case where source and sample are infinitesimal in size. Multiple elastic scattering and finite angular resolution reduce the variation of the observed elastic scattering yields with angle, but do not affect the integrated elastic cross section. At 1.63 MeV, elastically scattered neutrons that undergo a subsequent inelastic scattering thereby enter the inelastic detection channel and, since the inelastic scattering angular distribution is isotropic, they isotropically increase the magnitude of the measured inelastic angular distribution, fortuitously canceling the flux attenuation effect in that channel.

The Monte Carlo program MULCAT (Ref. 17) was used to correct the data for the above effects. Since the correction performed by MULCAT depends on the normalization of the uncorrected angular distributions, it was necessary to normalize the input to MULCAT realistically, as is now explained.

Flux attenuation by the scattering sample was determined by the analytic correction method of Cranberg and Levin[18] and the source-anisotropy effect was determined with the computer program FLUX.[19] These analytic methods indicated that the observed, angle-integrated scattering yield at both energies is 17—18 % smaller than that expected from the total neutron cross section measured by transmission methods.[3] Hence the measured elastic angular distributions, normalized to the total cross sections, were renormalized with a multiplying factor of 1/1.18 for the MULCAT input, while the normalized inelastic scattering angular distributions at 1.63 MeV were used without renormalization as MULCAT input, because of the cancellation of effects noted above. The consistency of this whole corrrection procedure is indicated by the fact that the Monte Carlo corrected results agreed with the measured total cross sections to within 2.5%, indicating a $\leq 2.5\%$ difference in normalization between Monte Carlo and analytically corrected cross sections. The differential cross sections reported herein are MULCAT corrected, but renormalized $\leq 2.5\%$ to agree precisely with transmission total cross sections averaged over the 100 keV energy range appropriate to these experiments. Although the renormalizations complicate correction procedures, they enable the use of accurate isotopic total cross sections as a standard for the normalization of differential cross sections. This results in a reduction in the systematic normalization uncertainty of the differential cross sections compared to what could be achieved by normalizing to scattering from hydrogen or carbon.

As a check on the Monte Carlo corrections, analytic angular dependence corrections were also carried out for $^{120}$Sn using a program written by Reber[20] and incorporating the methods of Blok and Jonker[21] for the multiple-scattering correction and the methods of Reber[20] and Harper[22] for the angular-resolution correction. Changes in the shape of the angular distribution for elastic scattering were about 30%. The analytically corrected angular distributions differed from the Monte Carlo corrected distributions by at most 22%, with the greatest differences occurring in the minima, and this agreement was considered to be quite satisfactory.

## IV. EXPERIMENTAL RESULTS

### A. Measured cross sections

The measured differential cross sections with all corrections are shown in Figs. 3—5. Relative uncertainties, e.g., those associated with the reproducibility of individual points, are 3—6 % and are smaller than the points on the graphs. The curves in Figs. 3 and 4 are complex potential fits with statistical model calculations for compound elastic scattering included for the elastic cross sections. In Fig. 5 the curves are statistical model calculations for the inelastic scattering cross sections, as discussed in Sec. V. Legendre polynomial fits were made in the form

$$\sigma(\theta)=\sum_i A_i P_i(\cos\theta)$$

to each angular distribution. Here $\sigma(\theta)$ denotes the appropriate differential scattering cross section and $P_i(\cos\theta)$ are the Legendre polynomials. The coefficients, $A_i$, are given in Table II. Figure 6 shows the elastic scattering Legendre polynomial fits to $^{116}$Sn and $^{124}$Sn for the two

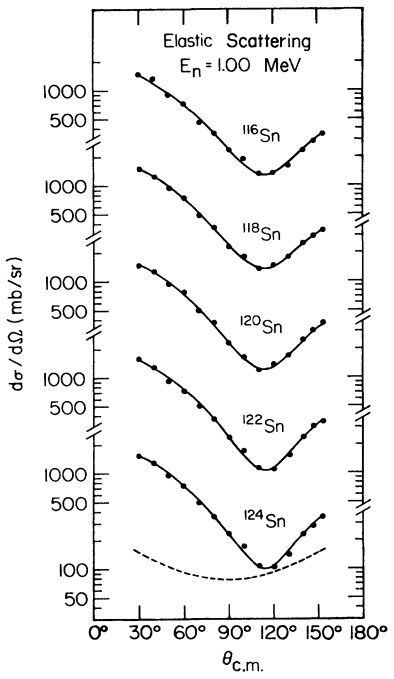


FIG. 3. Measured differential elastic cross sections for 1.00-MeV neutrons scattered by the isotopically enriched samples. The overall uncertainties are about the size of the data points. The solid curves are model calculations discussed in Sec. V. The dashed curve shows the compound elastic contribution for $^{124}$Sn, and is similar for the other isotopes.

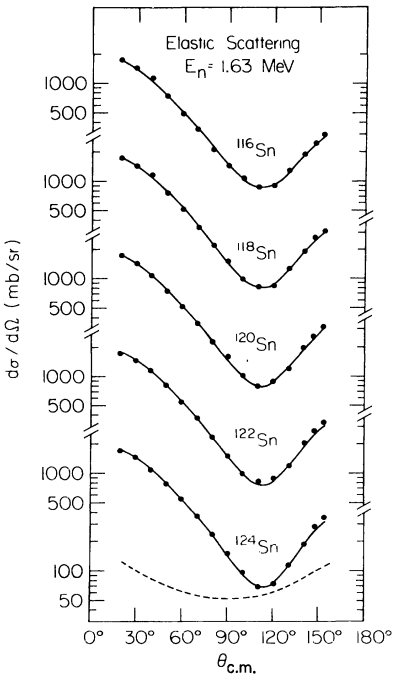


FIG. 4. Measured differential elastic cross sections for 1.63-MeV neutrons scattered by the isotopically enriched samples. The overall uncertainties are about the size of the data points. The solid curves are model calculations discussed in Sec. V. The dashed curve shows the compound elastic contribution for $^{124}$Sn, and is similar for the other isotopes.

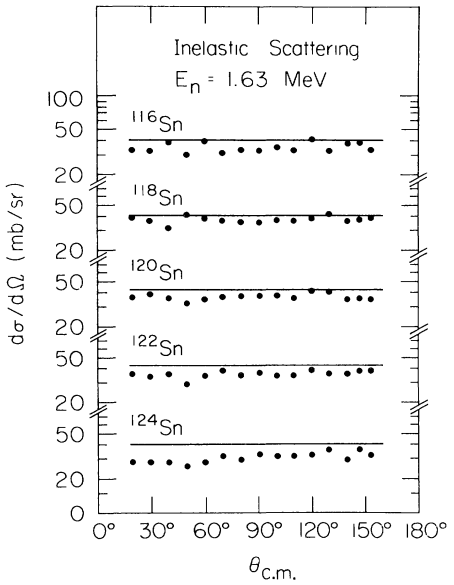


FIG. 5. Measured differential inelastic cross sections for 1.63-MeV neutrons scattered by the isotopically enriched samples. The overall uncertainties are about the size of the data points. The lines are statistical model cross sections discussed in Sec. V.

energies. It reveals the trend toward smaller cross section near the 115° minimum, and larger forward and backward angle cross sections as the neutron number $N$ increases. The differences are greatest in the minima, where the cross section decreases by $\approx$30% from $^{116}$Sn to $^{124}$Sn, while the increases at backward and forward angles are somewhat smaller. The Legendre polynomial fits for the other three isotopes lie in between the curves for $^{116}$Sn and $^{124}$Sn. The inelastic cross sections are almost isotropic and vary among the isotopes by as much as 22% in a manner that is not correlated with neutron number $N$.

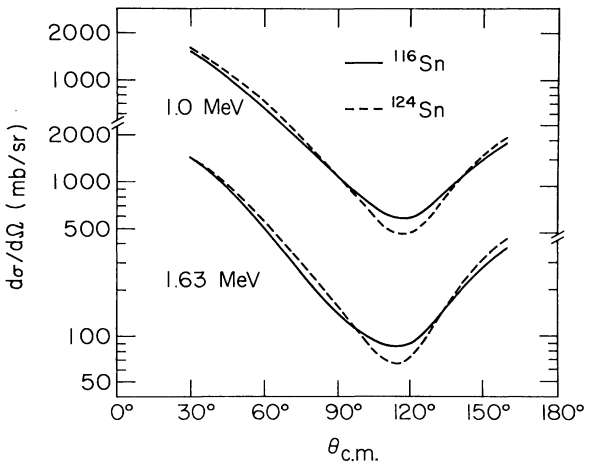


FIG. 6. Legendre polynomial fits to measured elastic differential cross sections for $^{116}$Sn and $^{124}$Sn at the two bombarding energies. The polynomial fits to data for the other three isotopes lie between these extremes.

TABLE II. Legendre polynomial expansion coefficients from least-squares fits to the center-of-mass experimental differential cross sections. Coefficients are given in mb/sr.

| Coefficient | Isotope 116 | 118 | 120 | 122 | 124 |
|---|---|---|---|---|---|
| 1.00-MeV elastic scattering | | | | | |
| $A_0$ | 509.0± 9.4 | 509.8± 6.8 | 516.9± 8.2 | 522.6± 8.3 | 518.7± 7.7 |
| $A_1$ | 645.0±22.0 | 643.8±16.1 | 654.3±19.1 | 679.8±19.8 | 680.1±17.8 |
| $A_2$ | 617.6±30.0 | 604.8±21.8 | 624.2±26.0 | 658.3±26.8 | 647.7±24.3 |
| $A_3$ | 113.9±28.2 | 92.8±20.0 | 67.2±22.6 | 94.9±24.0 | 82.0±22.2 |
| $A_4$ | 108.0±23.2 | 65.5±16.4 | 61.4±18.7 | 110.8±19.8 | 108.8±18.4 |
| 1.63-MeV elastic scattering | | | | | |
| $A_0$ | 424.0± 4.3 | 426.9± 3.8 | 425.5±2.9 | 435.4± 3.7 | 438.2± 4.0 |
| $A_1$ | 595.4±10.0 | 591.1± 8.9 | 588.3±6.8 | 597.6± 8.5 | 601.8± 9.4 |
| $A_2$ | 676.4±12.7 | 673.7±11.3 | 666.3±8.7 | 666.7±10.8 | 682.4±11.8 |
| $A_3$ | 205.3±10.6 | 179.1± 9.5 | 169.4±7.2 | 156.9± 9.3 | 141.2± 9.7 |
| $A_4$ | 151.9± 9.2 | 149.8± 8.7 | 141.7±6.5 | 138.3± 8.6 | 150.7± 9.0 |
| 1.63-MeV inelastic scattering | | | | | |
| $A_0$ | 33.7± 0.8 | 37.1± 0.5 | 35.9± 0.6 | 34.8± 0.6 | 29.9± 0.7 |

Contributing to the uncertainties in the measured cross sections were counting statistics in main and monitor detectors, uncertainties in the geometrical corrections, and uncertainties in the total cross sections to which the differential cross sections were normalized. The sources of uncertainty and their estimated magnitudes are given in Table III. The total uncertainty is the root mean square (rms) of the relative and normalization uncertainties. For the elastic scattering cross section the average cross section uncertainty is 3.6%. In the angular region of $100° \leq \theta \leq 130°$ where the cross section is smallest, a few of the data points have uncertainties ranging from 4.5% to 6.4%.

### B. Comparisons with other measurements

Langsdorf *et al.*[7] and Lane *et al.*[8] have made extensive studies of differential neutron scattering cross sections up to 2.3 MeV bombarding energy on natural tin using $BF_3$ neutron detectors. More recently, Gilboy and Towle[9] have measured the 1 MeV differential scattering cross section of natural tin using the time-of-flight method. Since the elastic and inelastic scattering cross sections have not been measured for the odd-$A$ Sn isotopes which make up $\simeq$17% of natural tin, any comparison between the present results and the previous work is necessarily incomplete. For this reason, we have chosen to construct very simple-minded synthetic natural-tin angular distributions from our data by making an unweighted average of the $^{118}$Sn and $^{120}$Sn cross sections. This average cross section was chosen for comparison because it corresponds to an average mass number near that of natural tin. At 1.63 MeV we have added together the elastic and inelastic cross sections for the purpose of comparison, since the earlier experiments did not distinguish elastic from inelastic scattering. This averaged cross section is 5—10% higher

TABLE III. Sources of uncertainty in measured cross sections and estimated magnitudes in percent.

| | 1.00 MeV elastic | | 1.63 MeV elastic | | 1.63 MeV inelastic | |
|---|---|---|---|---|---|---|
| | Relative | Normalization | Relative | Normalization | Relative | Normalization |
| Main detector counting statistics | 1.5—4 | | 1.5—5 | | 3.5—5.5 | |
| Monitor detector counting statistics | ≤1 | | ≤1 | | ≤1 | |
| Finite geometry correction | 2 | 0 | 2 | 1 | 3 | 3 |
| Transmission $\sigma_T$ value | | 1.0 | | 1.5 | | 1.5 |
| Relative efficiency | | 0 | | ≤0.3 | | 3 |
| rms | 2.7—4.6 | 1.0 | 2.7—5.5 | 1.8 | 4.7—6.3 | 4.5 |
| Total uncertainty | 2.9—4.7 | | 3.2—5.8 | | 6.5—7.7 | |

than the previous results at the forward and backward angles but agrees well around 90°. The agreement is acceptable, considering the crudity of the comparison.

## V. THEORETICAL ANALYSIS

The corrected elastic scattering angular distributions and the total cross sections from Ref. 3 at 1.00 and 1.63 MeV were fitted with an incoherent sum of shape-elastic scattering calculated with a complex potential and compound-elastic scattering calculated from a statistical model. The complex potential used for the calculations was

$$V(r)=-Vf(r)-iWg(r)-U_{so}h(r)\vec{l}\cdot\vec{\sigma}\ ,$$

where the real potential has a Woods-Saxon form, the imaginary potential has a Woods-Saxon derivative form, and the spin-orbit (so) potential is real with a Thomas form, i.e.,

$$f(r)=\{1+\exp[(r-r_0A^{1/3})/a]\}^{-1}\ ,$$

$$g(r)=4a'\frac{d}{dr}\left|\{1+\exp[(r-r_0'A^{1/3})/a']\}^{-1}\right|\ ,$$

$$h(r)=\left[\frac{\hbar}{m_\pi c}\right]^2\frac{1}{r}\left|\frac{d}{dr}f(r)\right|\ .$$

At these low bombarding energies, compound nucleus contributions are expected to be large and especially evident in the minima of the angular distributions. At 1.63 MeV, with one level excited, the effects of level-width fluctuations on the compound nucleus cross section are strong, and the correction of Dresner[5] and Lane and Lynn[6] provided the best fits to the elastic and inelastic scattering cross sections; in fact, use of the correction was necessary in order to fit the elastic scattering in the cross section minimum near 115°.

Starting with

$$r_0=1.25\text{ fm}\ ,$$

$$r_0'=1.30\text{ fm}\ ,$$

$$a=0.65\text{ fm}\ ,$$

$$a'=0.40\text{ fm}\ ,$$

the geometric parameters were adjusted to give the best fits to the elastic scattering data only for $^{120}$Sn. The effect of a small change in each parameter on the calculated elastic scattering cross section was noted. Next, all parameters, including $V$ and $W$, were judiciously varied in pairs until approximate fits to all isotopes were obtained. The parameters were then refined by the iterative use of ALTE,[23] a Wolfenstein-Hauser-Feshbach[24,25] (WHF) statistical model code that includes a level-width fluctuation correction, and JIB,[26] an optical model code with a search routine, using a $\chi^2$ criterion for best fit. In fitting $^{120}$Sn it became apparent that the differences in the elastic scattering cross section, $\sigma_{el}(\theta)$, among the isotopes could be accounted for varying only $V$ and $W$. The geometry parameters finally decided upon were

$$r_0=r_0'=1.26\text{ fm}\ ,$$

$$a=0.58\text{ fm},\quad a'=0.40\text{ fm}\ ,$$

which we call set $A$.

In order to arrive at best fits for all five isotopes the geometries were fixed at the above values, $U_{so}$ was fixed at 5.5 MeV, and $V$ and $W$ were then scanned for each isotope in the ranges $45\leq V\leq 50$ and $2\leq W\leq 9$ MeV in 50 keV steps using the computer code ABACUS-II (revised) (Ref. 27) which calculates the total, shape elastic, and compound elastic scattering cross sections. The experimental uncertainties of the data points, including those of the total cross sections,[3] were used in calculating the reduced $\chi^2$, and the best fit at each energy (i.e., that with the minimum $\chi^2$) is shown in Figs. 3 and 4. The dashed lines for $^{124}$Sn indicate the contribution of compound elastic scattering, which predominates in the minima of the differential cross sections. Compound elastic cross sections are similar for the other isotopes. The minimum $\chi^2$ fits are very similar to the Legendre polynomial fits, differing from them at most by 4%. The fits to the total cross sections agreed with the measured values to less

TABLE IV. Real and imaginary well depth values that best fit the elastic scattering cross sections, and reduced $\chi^2$, for geometry sets $A$ and $B$. Also real well depths and $\chi^2$ for fixed $W$ for set $A$. $V$ and $W$ are given in MeV.

| | Set $A$ | | | Set $A$ | | | Set $B$ | | |
|---|---|---|---|---|---|---|---|---|---|
| $A$ | $V$ | $W$ | $\chi^2$ | $V$ | $\langle W\rangle$ | $\chi^2$ | $V$ | $W$ | $\chi^2$ |
| $E_n=1.00$ MeV | | | | | | | | | |
| 116 | 48.45 | 7.03 | 3.1 | 48.36 | 5.90 | 4.2 | | | |
| 118 | 48.03 | 7.02 | 1.1 | 47.72 | 5.90 | 2.2 | | | |
| 120 | 47.73 | 5.95 | 1.5 | 47.76 | 5.90 | 1.5 | | NA | |
| 122 | 47.26 | 5.23 | 2.1 | 47.59 | 5.90 | 3.5 | | | |
| 124 | 46.96 | 4.48 | 3.2 | 47.47 | 5.90 | 8.0 | | | |
| $E_n=1.63$ MeV | | | | | | | | | |
| 116 | 47.21 | 6.96 | 2.2 | 47.03 | 6.04 | 3.2 | 44.7 | 6.1 | 6.8 |
| 118 | 46.96 | 6.30 | 1.3 | 46.88 | 6.04 | 1.5 | 44.4 | 5.6 | 4.1 |
| 120 | 46.63 | 6.42 | 0.6 | 46.49 | 6.04 | 0.7 | 44.1 | 5.5 | 1.5 |
| 122 | 46.10 | 5.82 | 2.4 | 46.04 | 6.04 | 3.5 | 43.7 | 5.4 | 1.9 |
| 124 | 45.68 | 4.93 | 2.2 | 45.65 | 6.04 | 5.5 | 43.1 | 4.3 | 1.2 |

than 0.02 b, well within the experimental uncertainties of $\simeq\pm 0.08$ b. The resulting values of $V$, $W$, and reduced $\chi^2$ for the best fits to the individual isotopes are given in Table IV. The curves in Fig. 5 are inelastic scattering cross sections calculated from the statistical model using transmission coefficients determined from the potentials that best fit the elastic scattering.

The following procedure was used to determine the uncertainties in $V$ and $W$ for each isotope. In order to determine the effect of possible normalization errors on $V$ and $W$ the $^{120}$Sn cross sections were renormalized by factors of 1.010 and 1.018 corresponding to the estimated normalization uncertainties of 1.0% and 1.8% for the 1.00 and 1.63 MeV data, respectively, and were refitted, giving different $V$ and $W$ values. These fits were as good as those to the exact data for $E_n = 1.00$ MeV, both visually and according to $\chi^2$, and were only slightly worse at $E_n = 1.63$ MeV. The changes in $V$ and $W$ caused by renormalization were taken to be the normalization uncertainties in these parameters. Since the statistical uncertainties in the individual data points are random, it was assumed that they would cancel out in their effect on the shape (e.g., relative values) of the angular distribution, leaving only the 2% uncertainty in the finite geometry correction as the effective relative uncertainty in the angular distribution. Uncertainties in $V$ and $W$ due to the 2% shape uncertainty were determined by distorting the corrected $^{120}$Sn cross sections within this uncertainty and seeing how large a change in $V$ and $W$ was necessary to fit the distorted shape.

These normalization and relative uncertainties are given for $^{120}$Sn in Table V and were also assigned to $V$ and $W$ for each of the other isotopes because of the similarity in the cross sections. No uncertainties were determined for the geometrical parameters since they are related to the well depths by the well-known $VR^2$ and $Wa'$ ambiguities[28,29] and are not a unique set. Other "families" of geometrical parameters came close to fitting the data at one energy, but the set used above was the one closest to the Wilmore and Hodgson[30] values and also the one that best fit all the data. One example of these other geometries is discussed in Sec. V D.

### A. Imaginary well-depth variation

At both bombarding energies, the magnitude of the angle-integrated elastic scattering cross section was much more sensitive to $V$ than to $W$. Increasing $W$ increases $\sigma_{el}(\theta)$ at the forward and backward angles, and decreases $\sigma_{el}(\theta)$ in the minimum. An attempt was made at fitting the 1.0 MeV data for all isotopes by holding $W$ fixed at its value of 5.9 MeV for $A = 120$ and varying $V$, searching for the minimum $\chi^2$. The resulting values of $V$ and $\chi^2$ are given in the middle section of Table IV. The change in $V$ vs $A$ in this case is about half that obtained when $W$ was also allowed to vary. The $\chi^2$ values indicate substantially worse fits for isotopes 116, 118, 122, and 124 than when $W$ was varied. Similar fits to the 1.63 MeV angular distributions with $W$ fixed at 6.04 MeV also gave much poorer agreement with the data, although in this case the best-fit values of $V$ were almost identical to those found when $W$ was allowed to vary. Figure 7 shows the best fit for $^{124}$Sn with fixed $W$ at the two bombarding energies. It is clear that $W$ must vary with neutron number to avoid calculated fits well outside the uncertainties in the measurements.

TABLE V. Uncertainties $\Delta V$ and $\Delta W$ due to relative and normalization uncertainties in the elastic scattering cross sections.

| $E_n$ | Relative | | Normalization | | Total | |
|---|---|---|---|---|---|---|
| (MeV) | $\Delta V$ | $\Delta W$ | $\Delta V$ | $\Delta W$ | $\Delta V$ | $\Delta W$ |
| 1.00 | 0.06 | 0.15 | 0.20 | 0.01 | 0.21 | 0.15 |
| 1.63 | 0.10 | 0.06 | 0.15 | 0.45 | 0.18 | 0.45 |

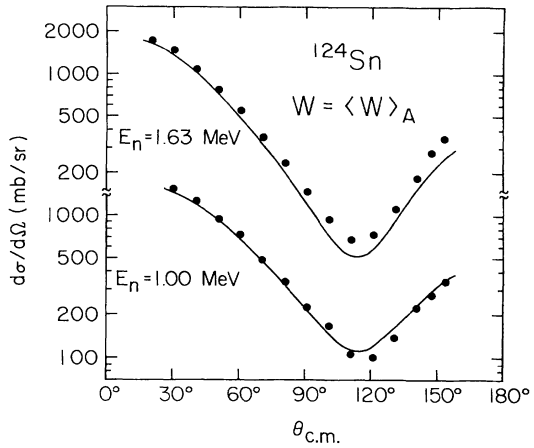


FIG. 7. 1.00- and 1.63-MeV cross sections for $^{124}$Sn. Also shown are the best theoretical fits that could be obtained by varying $V$ while holding $W$ fixed at its median value for the isotopic series at each bombarding energy.

### B. Neutron excess dependence of $V$ and $W$

Figure 8 shows the values of $V$ and $W$ for minimum $\chi^2$ plotted against the neutron excess, $\xi = (N-Z)/A$. $V$ and $W$ were parametrized as

$$V = V_0 - V_1\xi$$

and

$$W = W_0 - W_1\xi\ .$$

The lines in Fig. 8 are least-squares fits of these parametrizations to the values for each isotope and Table VI gives the best-fit parameter values, after being corrected for isotopic impurity, as discussed in the next paragraph. The fluctuations of the $V$ and $W$ values from the fitted straight line are consistent with the calculated uncertainties in $V$ and $W$, with the possible exception of the $W$ values at $E_n = 1.00$ MeV which show larger fluctuations for some unknown reason. From these fits it appears that a linear neutron excess dependence is a reasonable assumption for both $V$ and $W$.

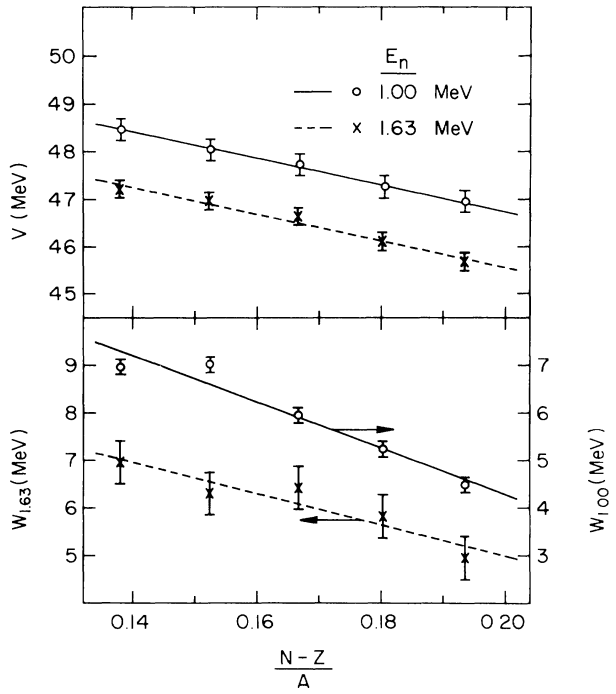


FIG. 8. The real and imaginary well depths $V$ and $W$ that gave the best fits to isotopic elastic scattering data at the two bombarding energies, versus neutron excess $(N-Z)/A$. The error bars are discussed in Sec. V B. The lines are linear least squares fits to the points.

The differences in the measured cross sections and in the resulting best-fit potentials for different scattering samples would be more pronounced had perfectly pure isotope samples been used. The samples averaged $\cong 5\%$ undesired Sn isotopes with insignificant amounts of other impurities. The average impurity mass number was $A=119.0$. To give an approximate correction for the effect of these impurities, values of $V_1$ and $W_1$ given in Table VI have been increased by 5% over the values derived from the least squares fit to the potential parameters derived from the data. After making this impurity correction, $V_0$ and $W_0$ were adjusted to give the same $V$ and $W$ for $^{119}$Sn as before the correction. The uncertainties in $V_0$, $V_1$, $W_0$, and $W_1$ were determined from fluctuations in the individual $V$ and $W$ values from the fitted straight lines.

TABLE VI. Real and imaginary well-depth parameters deduced from the best-fit well depths given in Table V. The parameters given below have been corrected for sample impurity, and are given in MeV. Uncertainties for the set $B$ analysis were not determined, but are expected to be about equal to those for set $A$.

| | 1.00 MeV | 1.63 MeV | |
|---|---|---|---|
| Parameter | Set $A$ | Set $A$ | Set $B$ |
| $V_0$ | 52.42±0.21 | 51.41±0.21 | 48.87 |
| $V_1$ | 28.6 ±1.6 | 29.5 ±1.6 | 29.36 |
| $W_0$ | 14.38±0.31 | 11.75±0.31 | 10.12 |
| $W_1$ | 51.0 ±3.7 | 34.1 ±7.0 | 28.54 |

It is interesting that the real well depths shown in Fig. 8 for the two bombarding energies differ by much more than their mutual uncertainties, implying an energy dependence which is much larger than is commonly found for global potentials.[4] Because of the small difference in energy and the fact that the number of open channels doubles in going from 1.00 to 1.63 MeV, this may be only a local effect which an average potential cannot be expected to represent. Recent work on sub-Coulomb-barrier proton scattering[31] has also found an anomalously large energy dependence of the real well depth.

### C. Radius dependence on $A$

In the analysis described above it was assumed that the relationship between the potential radius $R$ and the mass number $A$ is $R=r_0A^{1/3}$. This is a well-established relationship for large ranges of $A$. However, the results of electron scattering from the even-$A$ tin isotopes[32–34] indicate that the rms charge radius is proportional to $A^{1/6}$ for this isotope sequence. Taken together with the knowledge that the incident neutron will interact more strongly with the protons in the target than with the neutrons, this provided some impetus to analyze the present neutron scattering cross sections with a radial dependence on $A$ weaker than $A^{1/3}$.

The elastic cross sections presented here were therefore reanalyzed with optical potentials identical in form to the previous one except that the exponent of $A$ was taken successively to be 0.167 and 0.250. The radius $R$ for $^{120}$Sn was fixed at 6.213 fm, the same value used in the original analysis, and for each exponent of $A$, a radius parameter $r_m$ was derived such that $r_m(120^m)=6.213$ was satisfied. The radii for the other isotopes were then determined by the relation $R=r_mA^m$. The same diffuseness parameters as before were used, and $V$ and $W$ were varied to find the

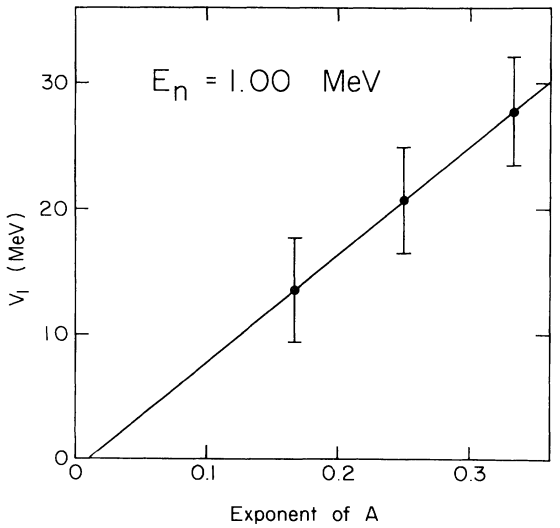


FIG. 9. The real well neutron-excess dependence term $V_1$ versus the exponent $m$ in the radius formula $R=r_mA^m$. The points shown are for $E_n=1.00$ MeV, but those for $E_n=1.63$ MeV are almost identical.

best-fit values for each isotope. The fits for $m < \frac{1}{3}$ are as good as those with $m = \frac{1}{3}$ and are therefore not shown. Sample impurity corrections were made in the same way as for $A^{1/3}$. The imaginary well depth $W$ was not significantly affected by the assumption of different exponents of $A$, i.e., $W_0$ changed by less than 0.1 MeV and $W_1$ by less than 0.8 MeV. However, the values of $V_1$ decreased by about half when the exponent was reduced from 0.33 to 0.167, as is shown in Fig. 9. This, of course, is quite consistent with the $VR^2$ ambiguity cited above. The change in $V$ from $^{116}$Sn to $^{124}$Sn leads to a $\Delta V/V \simeq -\frac{2}{47}$. For $R = r_0 A^{1/3}$, we find that $\Delta(R^2)/R^2 \simeq +\frac{2}{45}$. In other words if $R$ were held constant over the five isotopes, the neutron excess dependence would vanish.

### D. Analysis with other geometrical parameters

It was found that the 1.63 MeV elastic scattering data could also be fitted with another set of geometrical parameters, namely

$$r_0 = 1.28 \text{ fm},$$

$$r_0' = 1.32 \text{ fm},$$

$$a = 0.63 \text{ fm},$$

and

$$a' = 0.40 \text{ fm},$$

which we call set $B$. The overall quality of the fits is very nearly the same for set $B$ as for set $A$.

Table IV gives the best-fit well depths for geometry set $B$, and Table VI compares the parametrized well depths obtained with the two sets. The well depth parameters $V_1$ and $W_1$ derived with the two parameter sets agree within mutual uncertainties, but the $V_0$'s and $W_0$'s disagree badly.

Parameter set $B$ did not give acceptable fits to the 1.00 MeV cross sections, and hence must in some sense be thought of as spurious. Many other geometry sets were tested, but none were found that fit the whole isotope set at one bombarding energy as well as sets $A$ and $B$, much less at both 1.00 and 1.63 MeV.

## VI. DISCUSSION

The differential cross sections for neutron scattering by five even-$A$ isotopes of Sn have been measured with unusually high precision and accuracy at neutron energies of 1.00 and 1.63 MeV. The successive addition of four pairs of neutrons has been found to have a systematic effect on the elastic scattering differential cross section which is most pronounced in the minimum near 115°, where the cross section decreases $\cong 30\%$ with the addition of eight neutrons. At the forward and backward angles the effect of increasing the neutron number $N$ is to increase the cross section by a smaller percentage. Since the neutron shell is half filled for $^{116}$Sn, adding neutrons decreases the number of compound states at a given excitation energy. This is a possible interpretation of the decreasing compound elastic scattering with increasing $N$ which is obtained from the statistical model (WHF) calculations, and hence for the decrease in elastic scattering differential cross section in the cross section minimum as neutrons are added. The decrease in density of compound states is consistent with the increase in temperature with increasing $A$ deduced from the neutron evaporation spectra following bombardment of tin isotopes with 8.4 MeV neutrons.[22]

The elastic scattering cross sections have been fitted with a complex potential whose parameters could be determined with small uncertainties because of the high precision and accuracy of the measurements. The real and imaginary well depths of the potential were parametrized in terms of neutron excess as $V = V_0 - V_1\xi$ and $W = W_0 - W_1\xi$. $V_1$ is often interpreted as an isospin term because it is of about the same magnitude, but of opposite sign, for proton and neutron scattering.

From a global fit to neutron scattering data for 1 MeV $\leq E_n \leq$ 24 MeV and $56 \leq A \leq 209$, Bechetti and Greenlees[35] arrived at a global value of $V_1 = 24$ MeV, which is now more or less generally accepted. This is much smaller than the $V_1 = 50 \pm 10$ MeV obtained by Holmqvist and Wiedling[36] from analyzing 8 MeV neutron scattering from 22 elements in the range $27 \leq A \leq 209$. The value $V_1 = 29.0 \pm 1.6$ MeV found in the present work for the tin isotopic series at both $E_n = 1.00$ and 1.63 MeV agrees with the global result of Bechetti and Greenlees. It is 80% larger than the $V_1 = 16.1 \pm 2.3$ MeV found by Rapaport *et al.*[10] for the scattering of 11 MeV neutrons from these same tin isotopes with an analysis similar to ours. Makofske *et al.*[37] also obtained $V_1 = 16$ MeV from an analysis of proton scattering from even-$A$ tin isotopes at $E_p = 16$ MeV. However, Satchler[38] notes that if $^{112}$Sn were left out of their analysis, they would obtain $V_1 \cong 25$ MeV, which may show the effect of a subshell discontinuity. Except for the Holmqvist and Wiedling result, both global and local studies arrive at a value of $V_1$ in the range $21 \pm 5$ MeV for neutron scattering.

The effects on $V$ and $W$ of a change in dependence of $R$ on $A$ was also investigated in the present work. Figure 9 shows a plot of $V_1$ versus the exponent $m$ in the radius equation

$$R = r_m A^m$$

for $E_n = 1.00$ MeV. The points for $E_n = 1.63$ MeV are virtually the same and are not shown. From Fig. 9 we conclude that the generally accepted global value of $V_1$ and the global value of $m$, namely $\frac{1}{3}$, are barely consistent for the neutron potential of the even-$A$ tin isotopes. We cannot determine separately the value of either quantity, but for $V_1 = 24$ MeV, $m$ is limited to $0.24 \leq m \leq 0.34$. Furthermore, we find that $V_1$ is proportional to $m$, probably reflecting the $VR^2$ ambiguity, as noted above. Rapaport *et al.*[10] made a similar test of the effect of changing the $R$ vs $A$ dependence for their 11 MeV cross sections, and found that at that energy $V_1$ was independent of $m$. The imaginary potential was insensitive to the size of $m$ in both the present work and that of Ref. 10.

Good fits with a spherical optical model to the present data on the tin isotopes require $W_1 = 50.9 \pm 3.7$ and $34.1 \pm 7.0$ MeV at 1.00- and 1.63-MeV bombarding ener-

gies, respectively. This is in fairly good agreement with the $W_1$ values of 45 and 38 MeV determined for isotopic series of tin and selenium in coupled-channels analyses by Newstead and Delaroche[39] and by Lachkar *et al.*,[40] respectively.

On the other hand, a global value of $W_1 = 12$ MeV is given by Bechetti and Greenlees[35] for neutrons with energies up to 24 MeV. Rapaport *et al.*,[10] in their spherical optical model analysis of 11 MeV neutron scattering on the even-$A$ tin isotopes, find a $W_1$ which agrees with the global value. Thus, various studies are finding two different results for the dependence of $W$ on neutron excess, one set favoring the small value for $W_1$ expected on simple theoretical grounds[38] and another set of studies, including this one, suggesting values 3—4 times as large. It would appear that further work is necessary if the behavior of $W_1$, not to mention the validity of a linear dependence of $W$ on $\xi$, is to be understood.

At $E_n = 1.63$ MeV the differential cross sections for inelastic scattering to the $2^+$ first excited states are isotropic. After correction for isotopic impurities, the magnitudes of the inelastic cross sections for $A = 116$—$122$ are the same within their experimental uncertainties of $\simeq 7\%$, but for $^{124}$Sn, $\sigma$(n,n') is 13% lower than for the other isotopes.

It might be expected that in the present case, where scattering to only two levels is possible and where the potential parameters have been determined with high precision, that the statistical model[24,25] should provide a very good representation of the inelastic scattering cross sections. On the contrary, we find that the calculated cross sections are systematically higher than the experimental values by up to 20% (see Fig. 5). This is even more surprising when one considers the following:

(a) Even if the maximum possible Lane-Dresner level-width fluctuation correction factor[5,6] of 0.5 were applied to $\sigma_{n'}$, four of the five calculated cross sections would still be too high. The actual correction factor calculated by ALTE was $\simeq 0.55$.

(b) It has been shown by Moldauer[41] that applying only the level-width fluctuation correction results in an underestimate of the inelastic scattering cross section, since channel-channel correlations will cause an enhancement of $\sigma$(n,n') and hence will at least partially cancel the fluctuation corrections. In the present case, the inelastic scattering cross sections calculated with the fluctuation corrections are higher than the experimental values and inclusion of the channel-channel correlations would only make the disagreement with experiment worse, perhaps as much as 40%.

It would thus appear that there may be some inadequacy for this simple two level scattering problem either in the statistical model with all currently accepted corrections or with the assumption of a single, local potential.

## VII. CONCLUSIONS

A spherical optical model analysis has been made of the elastic scattering and total cross sections of 1.00 and 1.63 MeV neutrons from an isotopic series of nuclei with very similar nuclear structure. For each bombarding energy the best-fit values of $V$ show a good linear dependence on neutron excess, well within the experimental uncertainties, but the slope of the line depends strongly on the radius versus $A$ relationship. If a conventional mass-radius relationship is assumed, we find that a best fit to each nucleus results in a neutron-excess dependence of the real potential which is in good agreement with global studies of neutron and proton scattering at incident energies of 1—25 MeV. Furthermore, it is found that the real potential scattering strength, $VR^2$, is almost constant across the set of Sn isotopes at these bombarding energies.

We have found that a large neutron-excess dependence for the imaginary part of the potential is *absolutely* necessary to obtain satisfactory spherical optical model fits to the experimental cross sections. Varying the radius versus $A$ relationship does not affect the size of $W_1$. The best-fit values of the imaginary well depth, $W$, also show a fairly good straight line dependence on the neutron excess, $\xi = (N-Z)/A$. It is interesting to note that the sign of $W_1$ found here is negative, which is opposite to that usually found for proton scattering, and hence is consistent with an isospin interpretation of the variation of $W$ vs $\xi$.

The size of $W_1$ needed to satisfactorily fit the tin isotopes at these low neutron energies is 3—4 times larger than has been obtained in most global analyses, but is not inconsistent with the results of some other nucleon scattering studies covering limited regions of mass number. Large decreases in $V_0$ and in $W_1$ are found in the present work in going from $E_n = 1.00$ to 1.63 MeV. This may be related to the opening of the inelastic scattering to the first excited state, which represents a doubling of the number of open channels. If this is indeed the case, then the large $W_1$ values found here may not be inconsistent with the much smaller value found by Rapaport *et al.*[10] at $E_n = 11$ MeV.

## ACKNOWLEDGMENTS

The authors wish to thank Dr. M. T. McEllistrem for many invaluable discussions on the analysis of this data and Mr. S. P. O'Brien for helping with the optical model analysis, including evaluation of the uncertainties in the potential well depths. This work was supported in part by the National Science Foundation under Grants No. PHY 78-03209A02 and No. PHY 81-05572.

*Deceased.
[1]H. Feshbach, Annu. Rev. Nucl. Sci. **8**, 49 (1958).
[2]H. Feshbach, Ann. Phys. (N.Y.) **5**, 123 (1958); **19**, 287 (1962).
[3]R. W. Harper, T. W. Godfrey, and J. L. Weil, Phys. Rev. C **26**, 1432 (1982).
[4]C. M. Perey and F. G. Perey, At. Data Nucl. Data Tables **17**, 1 (1976).
[5]L. Dresner, Oak Ridge National Laboratory Report No. ORNL-CF-57-62-2, 1957 (unpublished).
[6]A. M. Lane and J. E. Lynn, Proc. Phys. Soc. London Sect. A

**70**, 557 (1957).
[7]A. Langsdorf, Jr., R. O. Lane, and J. E. Monahan, Phys. Rev. **107**, 1077 (1957).
[8]R. O. Lane, A. Langsdorf, J. E. Monahan, and A. J. Elwyn, Ann. Phys. (N.Y.) **12**, 135 (1961).
[9]W. B. Gilboy and J. H. Towle, Nucl. Phys. **42**, 86 (1963).
[10]J. Rapaport, M. Mirzaa, H. Hadizadeh, D. E. Bainum, and R. W. Finlay, Nucl. Phys. **A341**, 56 (1980); R. W. Finlay, J. Rapaport, M. H. Hadizadeh, M. Mirzaa, and D. E. Bainum, *ibid.* **A338**, 45 (1980).
[11]P. V. Vavilov, Zh. Eksp. Teor. Fiz. **32**, 320 (1957) [Sov. Phys.—JETP **5**, 749 (1957)].
[12]S. M. Seltzer and M. J. Berger, *Studies in Penetration of Charged Particles in Matter* (National Academy of Science—National Research Council, Washington, D.C., 1964), p. 187.
[13]F. D. McDaniel, J. D. Brandenberger, G. P. Glasgow, and H. G. Leighton, Phys. Rev. C **10**, 1087 (1974).
[14]Arthur Mittler, Ph.D. dissertation, University of Kentucky, 1970 (unpublished).
[15]William Galati, Ph.D. dissertation, University of Kentucky, 1969 (unpublished).
[16]H. Liskien and A. Paulsen, Nucl. Data Tables **11**, 569 (1973).
[17]D. E. Velkley, J. D. Brandenberger, D. W. Glasgow, and M. T. McEllistrem, Nucl. Instrum. Methods **105**, 519 (1972). MULCAT is the Monte Carlo code discussed in that paper.
[18]L. Cranberg and J. S. Levin, Los Alamos Scientific Laboratory Report No. LA-2177, 1959 (unpublished).
[19]F. D. McDaniel (private communication).
[20]J. D. Reber, Ph.D. dissertation, University of Kentucky, 1967 (unpublished).
[21]J. Blok and C. C. Jonker, Physica (Utrecht) **18**, 809 (1952).
[22]R. W. Harper, Ph.D. dissertation, University of Kentucky, 1980 (unpublished).
[23]W. R. Smith, Comput. Phys. Commun. **1**, 106 (1969); **1**, 181 (1969); Oak Ridge National Laboratory Report No. ORNL-TM-1117, 1965 (unpublished).
[24]L. Wolfenstein, Phys. Rev. **82**, 690 (1951).
[25]W. Hauser and H. Feshbach, Phys. Rev. **87**, 366 (1952).
[26]F. G. Perey, Phys. Rev. **131**, 745 (1963).
[27]E. H. Auerbach, Brookhaven National Laboratory Report No. BNL 6552, 1973 (unpublished).
[28]P. E. Hodgson, *Nuclear Reactions and Nuclear Structure* (Clarendon, Oxford, 1971), p. 156.
[29]P. Marmier and E. Sheldon, *Physics of Nuclei and Particles* (Academic, New York, 1970), p. 1111.
[30]D. Wilmore and P. E. Hodgson, Nucl. Phys. **55**, 673 (1964).
[31]B. Gyarmati, T. Vertse, L. Zolnai, A. I. Baryshnikov, A. F. Gurbich, N. N. Titarenko, and E. L. Yadrovsky, J. Phys. G **5**, 1225 (1979).
[32]A. S. Litvinenko, N. G. Shevchenko, A. Yu. Buki, G. A. Savitsky, V. M. Khvastunov, A. A. Khomich, V. N. Polishchuck, and I. I. Chkalov, Nucl. Phys. **A182**, 265 (1972).
[33]V. M. Khvastunov, N. G. Afanasyev, V. D. Afanasyev, I. S. Gulkarov, A. S. Omelaenko, G. A. Savitsky, A. A. Khomich, N. G. Shevchenko, V. S. Romanov, and N. V. Rusanova, Nucl. Phys. **A146**, 15 (1970).
[34]J. Ficenec, L. A. Fajando, W. P. Trower, and I. Sick, Phys. Lett. **42B**, 213 (1972).
[35]F. D. Bechetti, Jr. and G. W. Greenlees, Phys. Rev. **182**, 1190 (1969).
[36]B. Holmqvist and T. Wiedling, Nucl. Phys. **A188**, 24 (1972).
[37]W. Makofske, W. Savin, H. Ogata, and T. H. Kruse, Phys. Rev. **174**, 1429 (1968).
[38]G. R. Satchler, in *Isospin in Nuclear Physics,* edited by D. H. Wilkinson (North-Holland, Amsterdam, 1969).
[39]C. M. Newstead and J. P. Delaroche, in *Nuclear Structure Study with Neutrons,* edited by J. Erö and J. Scücs (Plenum, New York, 1974), pp. 387 and 470.
[40]J. Lachkar, M. T. McEllistrem, G. Haouat, Y. Patin, J. Sigaud, and F. Coçu, Phys. Rev. C **14**, 933 (1976).
[41]P. A. Moldauer, Phys. Rev. C **11**, 426 (1975); **12**, 744 (1975).